



Contents lists available at ScienceDirect

Science Bulletin

journal homepage: www.elsevier.com/locate/scibScience
Bulletin
www.scibull.com

Article

Quantitative analysis of the structural evolution in Si anode via multi-scale image reconstruction

Chen Zhu^{a,1}, Shiming Chen^{a,1}, Ke Li^a, Zu-Wei Yin^{b,*}, Yinguo Xiao^a, Hai Lin^{a,*}, Feng Pan^a, Luyi Yang^{a,*}^aSchool of Advanced Materials, Peking University Shenzhen Graduate School, Shenzhen 518055, China^bCollege of Energy, Xiamen University, Xiamen 361005, China

ARTICLE INFO

Article history:

Received 12 October 2022

Received in revised form 30 December 2022

Accepted 19 January 2023

Available online xxxx

Keywords:

Li-ion battery

Si anode

Structural evolution

Three-dimensional image reconstruction

ABSTRACT

Despite the high theoretical capacity, silicon (Si) anode suffers from dramatical capacity loss, due to its massive volume swings (up to 300%) during cycling. Hence, thorough understanding of the structural evolution mechanism is necessary and essential for performance optimization of Si anode. Herein, a multi-scale three-dimensional (3D) image reconstruction technique is firstly applied to visualize the structural evolution process of Si anodes. Three key components (Si particles, inactive components, and voids) in the electrode are quantitatively analyzed by focused ion beam and scanning electron microscope (FIB-SEM) technology. Furthermore, the average sizes of Si particles were run statistics during the cycling. By combining the componential observation within the electrode (macroscopic information) and the 3D models of the particle with solid electrolyte interphase (SEI) layer (microscopic information), the failure mechanism of Si anode is vividly demonstrated. This work establishes a new methodology to quantitatively analyze the structural and compositional evolution of Si anode, which could be further applied for the studies of many other electrode materials with similar issues.

© 2023 Science China Press. Published by Elsevier B.V. and Science China Press. All rights reserved.

1. Introduction

The continuous increasing demand of high-energy-density lithium-ion batteries (LIBs) has stimulated the development of high-capacity electrode materials [1–4]. Among a variety of promising candidates for anodes, silicon (Si) has drawn both academic and industrial interests due to its high theoretical specific capacity (3579–4200 mAh g⁻¹ for Li₁₅Si₄-Li_{4.4}Si), low redox potential (~0.4 V vs. Li/Li⁺), abundant resources and environmental benignity [5–7]. However, its large volume swing (~300%) upon lithiation/delithiation process leads to the pulverization of active materials and the continuous generation of unstable and thick solid electrolyte interphase (SEI) layer [8,9]. This, in turn, results in the electrode disintegration and rapid capacity fading.

It has been reported that the electrolyte additives are beneficial to form a more stable SEI layer, improving the cycling stability of Si anodes [10–12]. One of the most-investigated electrolyte additives is fluoroethylene carbonate (FEC) because of its significant effect on performance improvement of Si-based anodes, undergoing electrochemical reduction between 1.0 and 1.4 V (vs. Li/Li⁺) [13,14]. It

has been widely used as commercial sacrificial electrolyte components. In general, FEC can result in a SEI layer on Si anode with a higher concentration of lithium carbonate (Li₂CO₃) and lithium fluoride (LiF), which provides both enhanced mechanical strength and interfacial Li⁺ transfer [15–18]. In addition, the in-depth chemistry and dynamic morphological structure of SEI with FEC additive in Si anodes were studied by cryogenic electron microscopy and X-ray photoemission electron microscopy [19,20]. It has been found that FEC decomposes on the surface of Si particles, forming an organic polymerized vinylene carbonate layer, which could provide a buffer for the volume expansion of Si anodes.

The evolution of structural disintegration in electrodes is the key aspect for capacity fading of Si anodes. However, X-ray computed tomography allowing three-dimensional (3D) imaging of the interior for electrodes has the limitation of complex mathematical inversion procedures and reconstruction artefacts [21,22]. Alternatively, the transmission electron microscope (TEM) 3D reconstruction is more focused on particle analysis (nanoscale) [23,24]. Hence, based on the generation and rapid development of focused ion beam and scanning electron microscope (FIB-SEM) analysis technology, it has become a powerful tool for probing the structural evolution of macroscopic electrodes [25,26]. Importantly, FIB-SEM characterization technology is able to provide more detailed microscopic morphology information (e.g., porosity and particle size distribution), and chemical composition

* Corresponding authors.

E-mail addresses: yinzuwei@xmu.edu.cn (Z.-W. Yin), linhai@pkusz.edu.cn (H. Lin), yangly@pkusz.edu.cn (L. Yang).¹ These authors contributed equally to this work.

information when combined with energy dispersive spectroscopy (EDS) [27–29].

Herein, we applied FIB-SEM as an experimental protocol to analyze the change of bulk phase structure in Si anodes during cycling. Through the 3D image reconstruction technology, the dynamic interplay of Si particles and inactive components is analyzed visually and quantitatively. The result shows that FEC additive helps to reduce the pulverization of Si particles and the repeated formation of SEI, maintain the integrity of conductive networks in the electrode, thereby enhance the stability of Si anodes. By providing a clearer picture of the structural evolution in Si anodes from the perspective of electrode to particle, the proposed strategy might be suitable for other electrode systems.

2. Experimental

2.1. Materials

Polyacrylic acid was purchased from Aladdin. Micro-sized Si particles were kindly provided by Shanghai Shuitian Material Science Co. Ltd., and the anode electrolyte was obtained from DoDoChem. Freshly deionized water was used in experiments.

2.2. Preparation of electrodes

The Si anodes were made by a typical slurry casting method with active materials (Si), conductive carbon (acetylene black), and binder (polyacrylic acid) at a mass ratio of 6:2:2. The slurry was casted onto a copper (Cu) foil current collector and dried at 50 °C for 1 h. The electrodes were further dried in a vacuum at 100 °C overnight and cut into disks with a diameter of 10 mm. The typical mass loading of active materials on each electrode was $0.6 \pm 0.1 \text{ mg cm}^{-2}$, and the negative electrode was a bare lithium foil. The electrolyte was $1.2 \text{ mol L}^{-1} \text{ LiPF}_6$ in 1:1 (v:v) ethylene carbonate/diethyl carbonate with 10 wt% FEC or without 10 wt% FEC and the separator was porous polypropylene films (Celgard 2400).

2.3. Electrochemical measurements

The cycling tests were carried out using a Neware battery test system within the voltage range of 0.01–1 V (vs. Li/Li⁺) for the half cells. Cyclic voltammograms (CV) of the half cells were recorded at a scan rate of 0.1 mV s^{-1} . The electrochemical impedance spectra (EIS) experiments were performed on an CHI604E electrochemical station with a frequency range of 1 MHz to 0.1 Hz. Open-source MATLAB script-based software was used to calculate distribution of relaxation times (DRT) from the impedance data. Galvanostatic intermittent titration technique (GITT) was carried out under the current density of 0.05 C (1 C = 4200 mAh g^{-1}). Before GITT test, the battery had been cycled for 5 cycles. The pulse time and relaxation time were 10 and 30 min, respectively. Unless otherwise specified, all electrochemical measurements were conducted at room temperature in half cells.

2.4. Material characterizations

Field-emission scanning electron microscopy (ZEISS SUPRA[®] 55, Carl Zeiss) was used to observe the top-view morphology of as-prepared samples. Raman spectrometer (inVia Reflex) was used to analyze the material structure on surface of Si anodes under the argon atmosphere. The cross-section images of the electrodes were obtained using focused ion beam (FEI, Scios) equipment. The change in chemical state on the electrode surface was analyzed by X-ray photoelectron spectra (XPS) (ESCALAB 250Xi). All the

samples have been transferred in vacuum and the base pressure of sample chamber was kept below 3.0×10^{-10} mbar during XPS measurements. The conductivities of electrodes were measured with a four-probe method, using Keithley 4200-SCS semiconductor characterization system. The frozen section of sample was obtained by (Leica CM1950) equipment which was coated in resin.

2.5. 3D FIB-SEM image reconstructions

A FIB-SEM (FEI Scios-ZEISS SUPRA[®] 55) is a dual beam setup that combines an obliquely focused ion beam and a vertically scanned electron beam in one system, where the ion beam is used for milling and the electron beam is used for imaging. In order to avoid charging during SEM imaging and to protect the sample from ionic damage, the protective platinum layer ($\sim 0.5 \mu\text{m}$) was coated on the surface of sample, using an *in-situ* liquid metal organic ion source (LMIS) deposition. The 30 kV Ga⁺ beam and 1 nA beam current were used at normal incidence to locally cross-section the indentation sites, and SEM images were taken of each sequential 2D slice at a tilt angle of 52° by T1 mode. The repetitive imaging and slicing process were automatically controlled using Auto Slice and View software (FEI, Scios), and the spacing between adjacent 2D slices was 50 nm. After collecting cross-sectional images of each sample, alignment, segmentation, cropping, and labeling of 3D reconstructions were performed by Avizo software. The dimensions of the reconstruction model for Si anodes are $x = 25 \mu\text{m}$, $y = 12 \mu\text{m}$, and $z = 7.5 \mu\text{m}$. Avizo was also used to quantify various microstructural features of the 3D reconstruction of the sample (the volume and surface area of each phase and porosity calculation). The Segmentation module was used to segment different parts of the reconstruction model which was calculated by using the Volume Fraction module subsequently. Multi-thresholding segmentation is an alternative way of segmentation that may require less manual interaction, but it typically requires the higher quality images. Under favorable conditions, a satisfying segmentation can be achieved automatically based solely on the gray values of the image data. This is done by classifying the voxels into foreground and background voxels on the basis of their intensities or voxel values to separate the object from the background. With this procedure, each voxel value lower than the threshold is assigned to Exterior and each voxel value greater than or equal to the threshold is assigned to Inside. However, this may cause voxels to be labeled that are not part of the object but have voxel values above the threshold. Set the remove couch option to suppress it, which assures that only the largest coherent area will be labeled as the foreground (Inside) and all other voxels are assigned to the background (Exterior). As shown in the Fig. 1, the detailed image reconstruction process is explained according to the operation procedure.

Image collection. The T1 detector is primarily designed to collect backscattered electrons and provides composite sample contrast. And the contrast of backscattered electron imaging is caused by the difference of atomic number, so the backscattered electron is generally used to distinguish different phases. Therefore, the T1 mode was used for acquisition of electron beam images at the early stage of this 3D reconstruction, the different components could be identified and segmented according to image contrast.

Image data import. Firstly, a series of TIFF images obtained according to the Auto Slice&View4 are imported, and the images were set at 52° tilt (the angle between the FIB ion beam and the focal plane). The voxel size was calculated according to the image pixels and the horizontal field width (HFW) of the image (voxel size = HFW/width pixel point), so as to determine the model size of the Si anodes in Avizo.

Align slices. Since there is a 52° inclination between the sample platform and the horizontal plane during ion beam milling, with

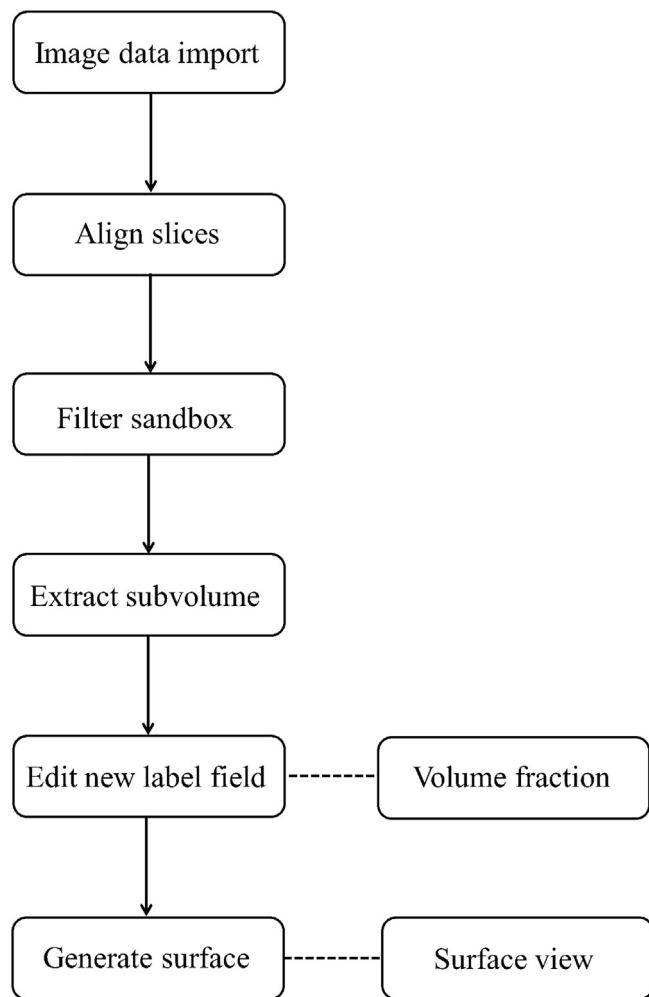


Fig. 1. The diagram about the process of image reconstruction for Si anodes.

the depth of Z direction, the image imaged under the electron beam will tilt upward, it is necessary to align the imported image before image processing. According to the details of the images, they were recognized and aligned.

Filter sandbox. Due to the uneven milling of ion beam, the curtain effect appears in the images. The filter sandbox module provided by Avizo can effectively eliminate the curtain effect and improve the sample image quality. In this experiment, FFT filter mode was selected for image noise reduction.

Extract subvolume. Because of the large size range of original images, which is not appropriate to the image construction of 3D models, the volume of the intermediate region was extracted from the Si anodes by extract subvolume module. For the convenience of subsequent analysis and comparison, the dimensions of the reconstruction model for Si anodes are $x = 25 \mu\text{m}$, $y = 12 \mu\text{m}$, $z = 7.5 \mu\text{m}$ uniformly.

Edit new label field. In order to characterize the spatial distribution of each component in the Si anodes clearly, edit new label field module was used to characterize the whole model in blocks. In this experiment, the model was divided into three parts, namely Si particles, inactive components, and voids, which is assigned red, blue, and green, respectively. The segmentation module was used to extract different components. The thresholding tool was used to divide the components according to different image thresholds on a large scale, and the details were refined by the brush tool.

Volume fraction. According to the three parts divided by the edit new label field module, volume fraction, a calculation tool, can calculate the volume fraction of each component.

Generate surface. This module can transform image data into visual three-mode models.

Surface view. This module can show the whole 3D model and the separate components clearly.

Particle fragment reconstruction. On the basis of electrode reconstruction, the extract subvolume module was used to narrow the range of interest to around particle, and then the segmentation module in the edit new label field module was used to extract target particle. Based on the contrast of the image, the brush tool was used to calibrate the boundary part.

3. Results and discussion

3.1. Electrochemical behavior of Si anodes

The galvanostatic cycling tests of Si anodes in $1.2 \text{ mol L}^{-1} \text{ LiPF}_6$ in 1:1 (v:v) EC/DEC with 10 wt% FEC (referred as Si-10% FEC) or without FEC (referred as Si-0% FEC) are carried out to evaluate their electrochemical performance. As shown in Fig. 2a and Fig. S1 (online), Si-10% FEC exhibits an initial discharge capacity of 3821 mAh g^{-1} which is higher than that of Si-0% FEC (3510 mAh g^{-1}). The extra capacity derives from the formation of SEI [17]. Additionally, the Coulombic efficiency of Si-10% FEC anodes is much higher and smoother during the continuous cycling process, which could be ascribed to the formation of a relatively stable SEI layer. Under 0.2 C, the Si-10% FEC anodes achieved a specific capacity of 2312 mAh g^{-1} after 100 cycles, corresponding to a capacity retention of 68.7%; by contrast, the capacity of Si-0% FEC anodes rapidly faded to 1154 mAh g^{-1} after 100 cycles, which is only 40.1% of the initial capacity. Such a difference in cycling stability is attributed to the formation of a relatively stable SEI layer in Si-10% FEC anodes [19]. A close observation shows that the capacity decay of Si-0% FEC anodes accelerated after about 30 cycles. Therefore, in the subsequent image reconstruction study, the Si anodes after 1, 30, and 100 cycles were chosen as research objects to analyze the structural evolution, respectively.

Moreover, the results of rate performance (Fig. S2 online) show that Si-10% FEC anodes possess superior rate capability over Si-0% FEC anodes. This result can be attributed to the higher Li^+ diffusion coefficient in Si-10% FEC than that in Si-0% FEC at different state of charge (Fig. S3 online). Then, the initial cyclic voltammetry curves of Si-10% FEC and Si-0% FEC anodes were compared in Fig. S4 (online), where the reduction peak at $\sim 1 \text{ V}$ corresponds to the decomposition of FEC [13]. Consequently, a large amount of LiF was generated on the surface of Si-10% FEC anodes after cycling as demonstrated by the XPS (Fig. S5 online). In addition, the O 1s spectra displays an obvious characteristic peak (lattice O) only for the Si-0% FEC anodes at 529 eV, which can be explained by the formation of Li_2O and exposed Si particles with oxide layer on the surface [30]. This result also agrees with the scanning electron microscope (SEM) images (Fig. S6 online), where the fragmented Si particles were scattered on the surface of the electrode. In the contrary, a relatively homogeneous and stable layer was formed on the surface of Si-10% FEC anodes and the difference became more evident after 100 cycles.

Next, combining the EIS and DRT profiles before cycling, FEC additive is revealed that benefits to improve the Li/electrolyte charge transfer (Fig. S7 online). As shown in Fig. 2b and c, the Li^+ migration resistance (R_{SEI}) and charge-transfer resistance (R_{ct}) of the Si-0% FEC anode increase significantly during cycling. The internal resistances of the Si-10% FEC anode (2.3, 3.8, and 10.9Ω corresponding to 1st cycle, 30th cycle, and 100th cycle,

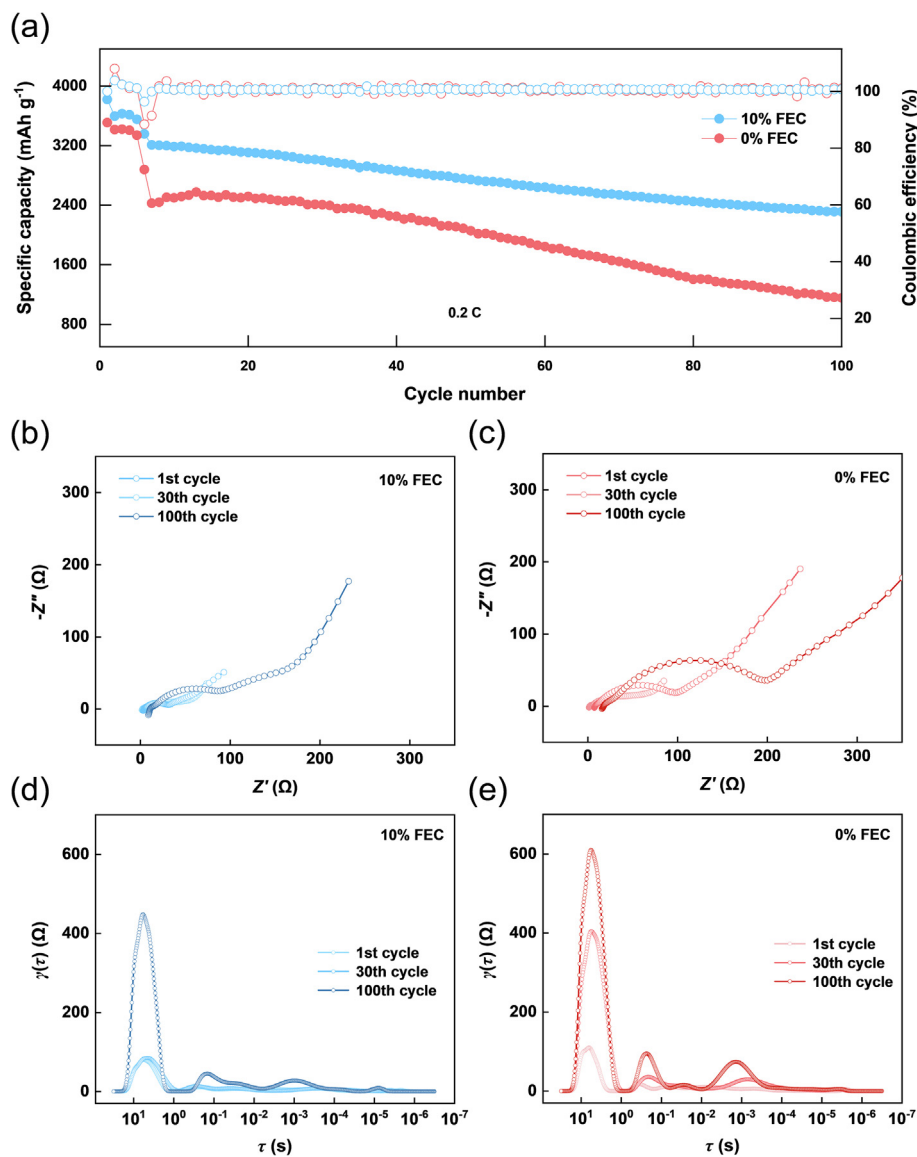


Fig. 2. The electrochemical behavior of different Si anodes. (a) Cycling performance and Coulombic efficiency of Si anodes with 10% FEC or without FEC (0% FEC) in the electrolyte at a rate of 0.05 C for the first 5 cycles and 0.2 C for the subsequent cycles. Electrochemical impedance spectra (EIS) of Si-10% FEC anodes (b) or Si-0% FEC anodes (c) after 1, 30, 100 cycles. Distribution of relaxation times (DRT) profiles of Si-10% FEC anodes (d) or Si-0% FEC anodes (e) after 1, 30, 100 cycles.

respectively) are measured to be lower than those of the Si-0% FEC anode (2.5, 8.1, and 17.5 Ω corresponding to 1st cycle, 30th cycle, and 100th cycle, respectively). Different peaks in DRT profiles could be clearly identified to present the electrochemical processes in the cell and the impedance of various processes is quantified based on the peaks [31,32]. The DRT profiles (Fig. 2d and e) also exhibit an obvious characteristic peak (corresponding to SEI) for the Si-0% FEC anodes from 10^{-4} to 10^{-2} s, which suggests that the continuous formation of a thick SEI on the surface of Si particles through consuming the electrolyte; while such increase can hardly be observed for Si-10% FEC [33–35]. Besides, very little difference can be observed from the EIS and DRT results of Si-10% FEC anodes between 1st and 30th cycles, indicating a well-maintained conductive network due to the highly stable electrode structure.

3.2. Reliability validation of image reconstruction

To reconstruct a 3D large-scale electrode internal model, auto-slicing and cross-section reconstruction technique were employed

to sequentially slice electrodes under different cycling states (more detail information in Experimental section). Before the FIB auto-slicing process, a protective platinum layer (~ 0.5 μm) was coated on the surface of Si anode to protect the sample from ionic damage. Also, the beam current was set to 1 nA, which is available to obtain a morphologically intact sample within a reasonable time. The scanning zone of SEM was corrected automatically during FIB cutting processes, by using Auto Slice and View software to recognize the cross-correlation of features on the surfaces of the Si anodes. The sequential two-dimensional (2D) slices of Si anodes under different electrochemical status were shown in Fig. S8 (online), where Si particles can be clearly distinguished. Video S1 (online) demonstrates a complete slicing process in the part of Si anodes. To preclude the thermal effect of ion beam on Si anodes, we made a comparison of the sample prepared by the 2D slice using FIB (1 nA) with that obtained from cryo-ultramicrotomy. As shown in Fig. S9 (online), there was no significant difference between the slice cut by FIB 1 nA ion beam and the mechanically sliced sample. After collecting cross-sectional images of Si anodes by SEM,

alignment, segmentation, cropping, and labeling of 3D reconstructions were performed by Avizo software [36,37]. The interactive multi-threshold segmentation was applied for consecutive images, benefiting to the calculated microstructural parameters subsequently [38,39]. It is mainly based on the difference of image contrast to identify the components, which is further verified by EDS analysis (Fig. S10 online). Observing the cross-sectional image, except for the voids, the areas with relatively shallow contrast are Si particles, while the darker areas are inactive components (i.e., conducting agent, binder, and SEI). To test the reliability of this method and reduce reconstruction errors, the componential distribution of a pristine Si anode is quantitatively analyzed (Fig. S11 (online) and Table 1). As a result, the percentage of each component content calculated from the reconstruction model coincides with the pristine electrode components, indicating high credibility in identifying different components. Moreover, the high resemblance of a remodeled pristine Si particle to a real one (Fig. S12 online) strongly confirms the reliability of this method in single-particle modeling.

3.3. Image reconstruction of Si anodes

As shown in Fig. 3, the 3D structure of Si anodes can be obtained in Fig. S8 (online), where could be divided into Si particles (red),

Table 1

Volume percentage of each component in the reconstruction model and real anodes before cycling.

Type	Volume percentage (model)	Volume percentage (reality)
Si particles	60.0%	60.0%
Inactive components	36.3%	40.0%
Voids	3.70%	/

inactive components (blue), and voids (green). Comparing Fig. 3, it can be seen that in a fixed space, higher volume percentage of Si particles can be observed from the reconstructed models of Si-10% FEC anodes. At the same time, more voids were generated in the Si-0% FEC anodes which damage the integrity of conductive networks. In this view, FEC additive helps to stabilize the structure of Si electrode in the discharge/charge process. This finding is in accordance with the cross-sectional thickness of Si electrodes observed by SEM (Fig. S13 online). The thickness of pristine Si electrode (11.7 μm) exhibits different degrees of expansion in 10% FEC (16.4 μm) and 0% FEC (25.63 μm) electrolytes after 30 cycles. The result manifests that the addition of FEC has a good inhibitory effect on the volume expansion of Si electrodes. With such large volume expansion, the active material content will be diluted

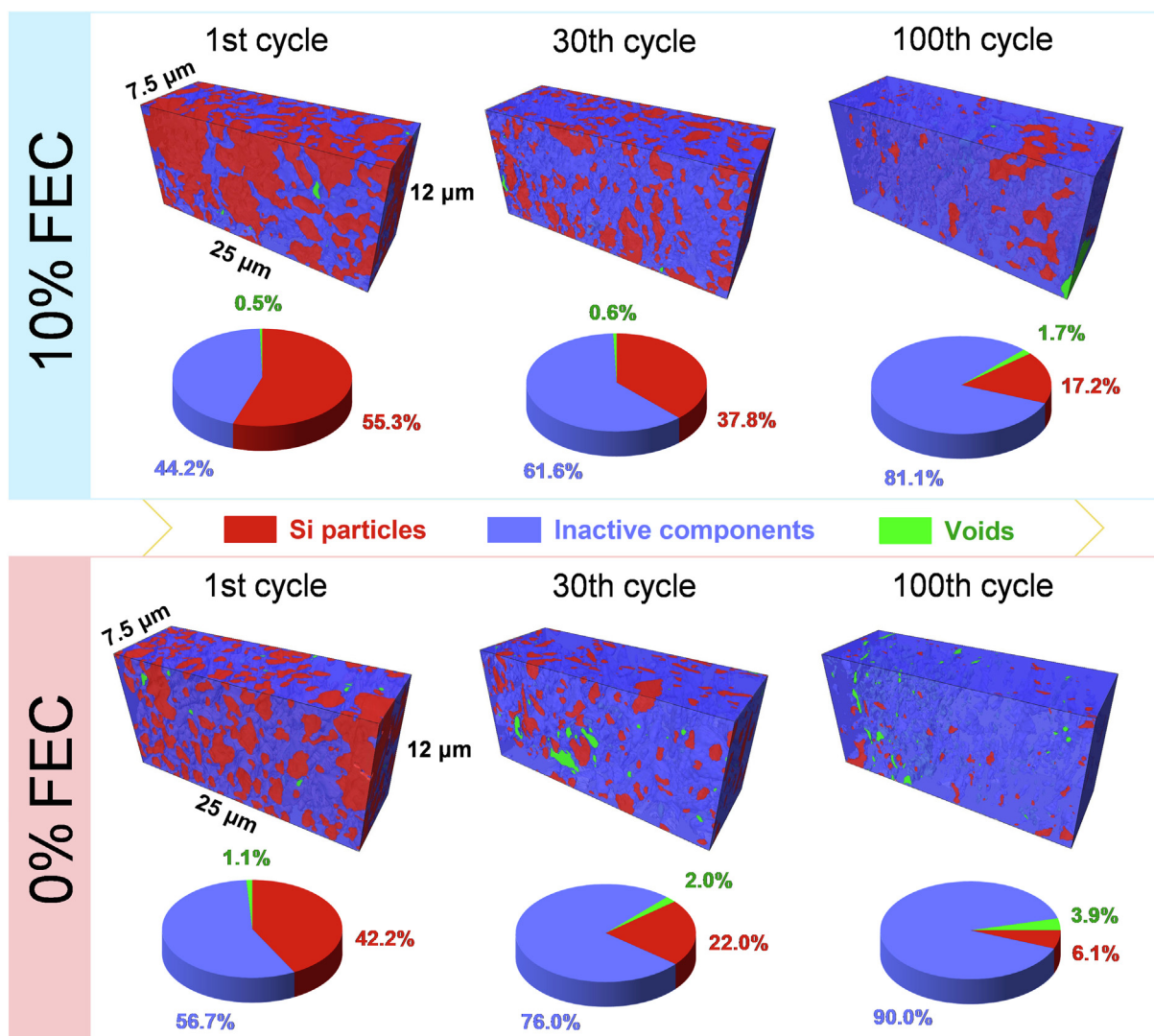


Fig. 3. 3D image representation of Si anodes under different electrochemical status: in the 10% FEC-containing electrolyte (up) and in the FEC-free electrolyte (down).

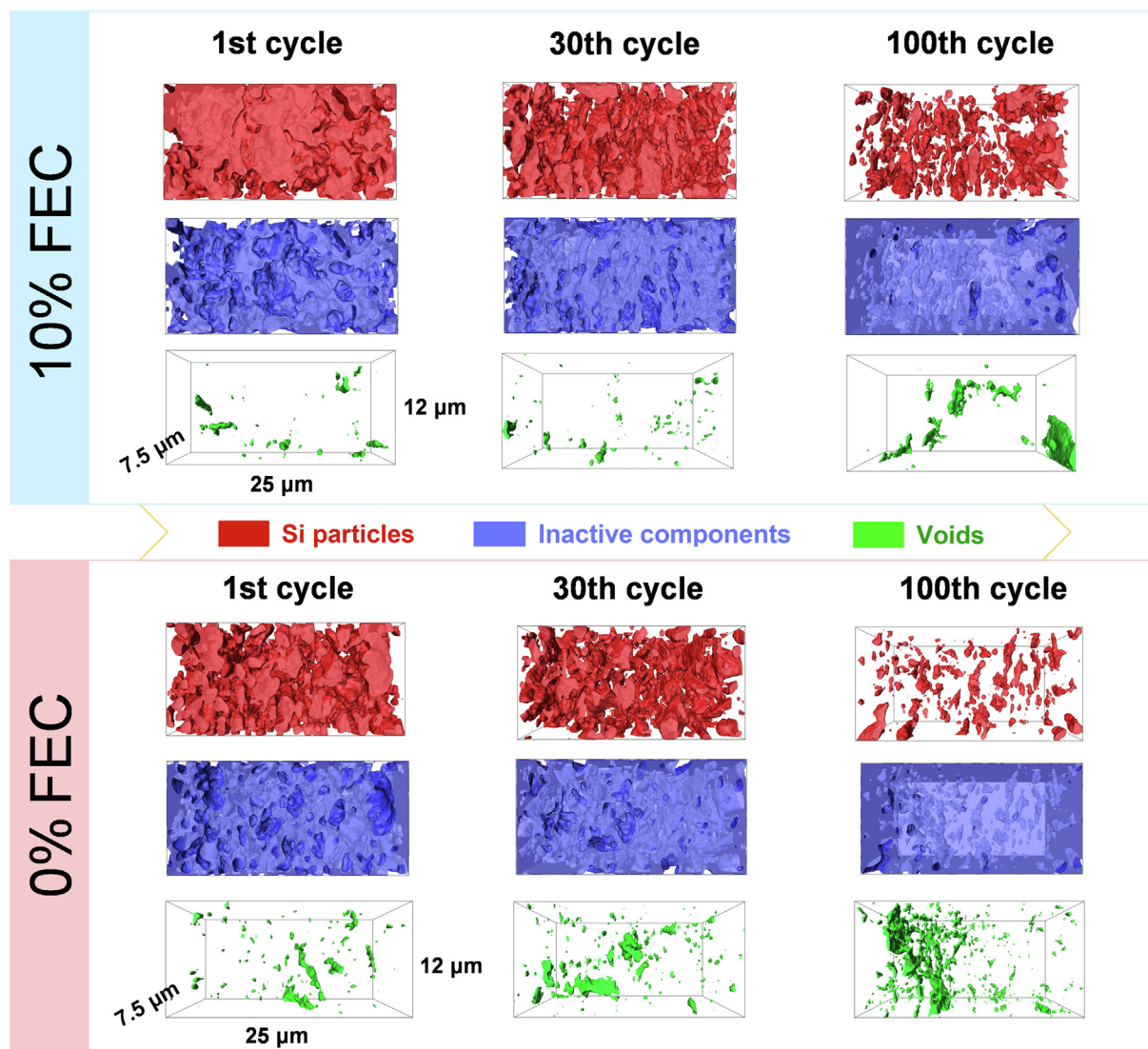


Fig. 4. 3D representation of the Si particles, inactive components, and voids using multi-threshold segmentation: in the 10% FEC-containing electrolyte (up) and in the FEC-free electrolyte (down).

within a fixed space. This finding explains the sharp capacity fading of FEC-free Si anodes: as the distance between active particles increases, the limited amount of conductive agent in inactive components is also diluted continuously, which is unable to provide an effective conductive network, resulting in rapid capacity fading. The Si-10% FEC anode also clearly exhibits a much lower areal resistivity ($6.06 \Omega \text{ m}$) compared with the Si-0% FEC electrode ($18.18 \Omega \text{ m}$) after 30 cycles, which could be attributed to the relative integrity of the conductive network (Fig. S14 online).

Additionally, the volume percentage of each component in Si anodes is quantitatively measured (Fig. 3). After 1st cycle, the Si-10% FEC anodes contain 55.3% active material of the total components. In contrast, the content of the active material in Si-0% FEC anodes rapidly faded to 42.3%. After 100 cycles, active material in Si-10% FEC still takes up 17.2% of the electrode whereas only 6.1% of Si is remained in Si-0% FEC. The gradually increasing inactive components in both electrodes suggest a thickening process of the SEI layer on the surface of Si particles, which originates from either electrolyte decomposition or the formation of electrochemically inactive lithium silicate [40].

In order to observe the evolution of each component clearly, they were extracted separately through multi-threshold segmenta-

tion technology from the models (Fig. 4). The particles in active materials continuously disintegrated from micro-size to nano-size and a part of fragmented Si nanoparticles are gradually embedded and merged into the inactive components. From the Raman spectroscopy (measured under argon atmosphere) of Si anodes, it could be seen that the amorphous Si signal appears in Si-0% FEC anodes after 100 cycles (Fig. S15 online). These results further confirm that the SEI on Si-0% FEC anode fails to fully passivate Si surface.

3.4. Image reconstruction of Si particles

Apart from the macroscopic structure evolution, the 3D structure of a single Si particle could also be obtained through the developed 3D image reconstruction technology (Fig. 5), where its bulk (red) can be differentiated from its SEI (blue). Based on the difference in image contrast between Si particles and SEI, reconstruction models are divided by the segmentation module (more details in Experimental section). After the first cycle, a thin SEI layer was generated around the Si particle. As cycling continues, a relatively thick yet dense SEI was formed on the surface of Si-0% FEC particle (Fig. 4), accompanied with rapid decay of capacity. Besides, Si par-

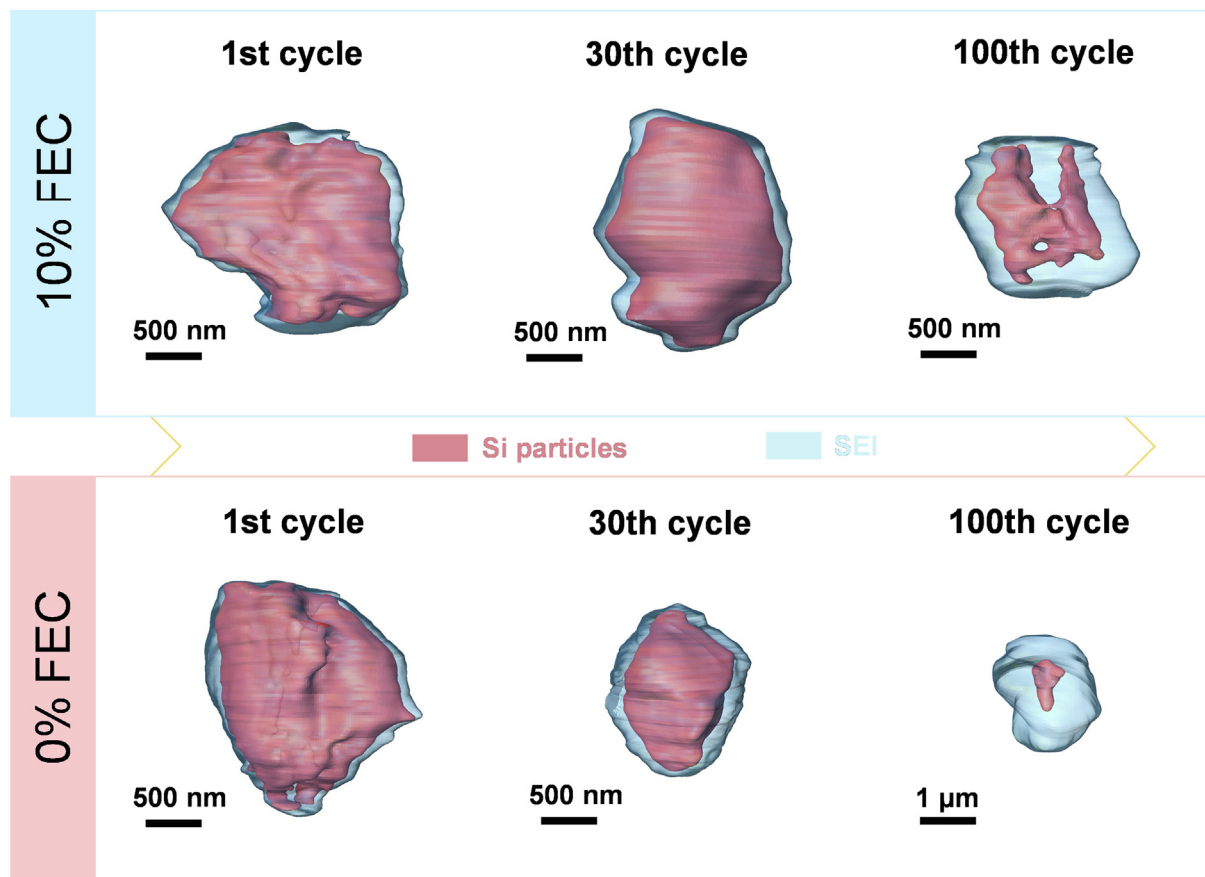


Fig. 5. 3D representation of Si particles and their SEI under different electrochemical status: in the 10% FEC-containing electrolyte (up) and in the FEC-free electrolyte (down).

Table 2

The measurement of Si particles size under different electrochemical status in the reconstruction models.

Average size (μm^3)	Pristine	1st cycle	30th cycle	100th cycle
Si-10% FEC	5.62	5.32	5.20	2.37
Si-0% FEC		5.11	3.51	0.84

ticles gradually pulverized and lost their electrochemical activity during the cycling. The fluctuant Coulombic efficiency during sequential cycles also suggests that excess SEI was accumulated on the surface of broken Si particles continuously until complete pulverization (Fig. 2a). By contrast, with the help of FEC, the “aging” process of SEI can be suppressed. As displayed in Fig. 5, Si particle and SEI almost maintain their initial size and shape after 30 cycles in the Si-10% FEC anode. With long-term cycling, the thin yet robust SEI grows slightly thicker, acting as a “protective shell” and restrains the pulverization of Si particles.

Table 2 shows the statistical results of the average particles sizes in different Si electrodes. It is obvious that the Si particles continuously broken corresponding to the reduction of size. Additionally, the particles of Si-10% FEC anodes gradually pulverized from $5.32 \mu\text{m}^3$ (corresponding to the 1st cycle) to $2.37 \mu\text{m}^3$ (corresponding to the 100th cycle); while more drastic pulverization can be observed in Si-0% FEC anodes (from 5.11 to $0.84 \mu\text{m}^3$). This further illustrates that the existence of FEC is helpful to reduce the pulverization of Si particles and form a stable SEI, which improves the electrochemical performance of the anodes. Furthermore, Si particles barely pulverized in the Si-10% FEC anode during 30 cycles. These results are in good accordance with the EIS and the DRT profiles of Si-10% FEC anodes after 30 cycles (Fig. 2b and d),

manifesting the conductive network of the electrodes was not damaged.

3.5. Effect of electrolyte additive FEC on structural evolution of Si anodes

A combination of the above image reconstruction techniques and EIS, SEM, XPS, EDS, Raman reveals a vivid landscape for the interplay between Si particles and SEI during cycling (Fig. 6). Without FEC additive, drastic pulverization of Si particles is observed, leading to electrode disintegration eventually. In addition, the repeated SEI destruction and generation process on the surface of pulverized Si particles cause continuous accumulation of SEI, blocking the charge transfer pathways. Whereas in the presence of FEC, both the integrity of electrode and the average size of Si particles are better retained after cycling, indicating mitigated SEI growth and particle pulverization. In this view, inert LiF is helpful to construct a thin and robust SEI [41,42]. Under the promotion of FEC sacrificial additive, it is easier to construct a LiF-rich SEI which contributes to maintaining a dynamic equilibrium between active materials and SEI, improving the electrochemical performance of Si anodes.

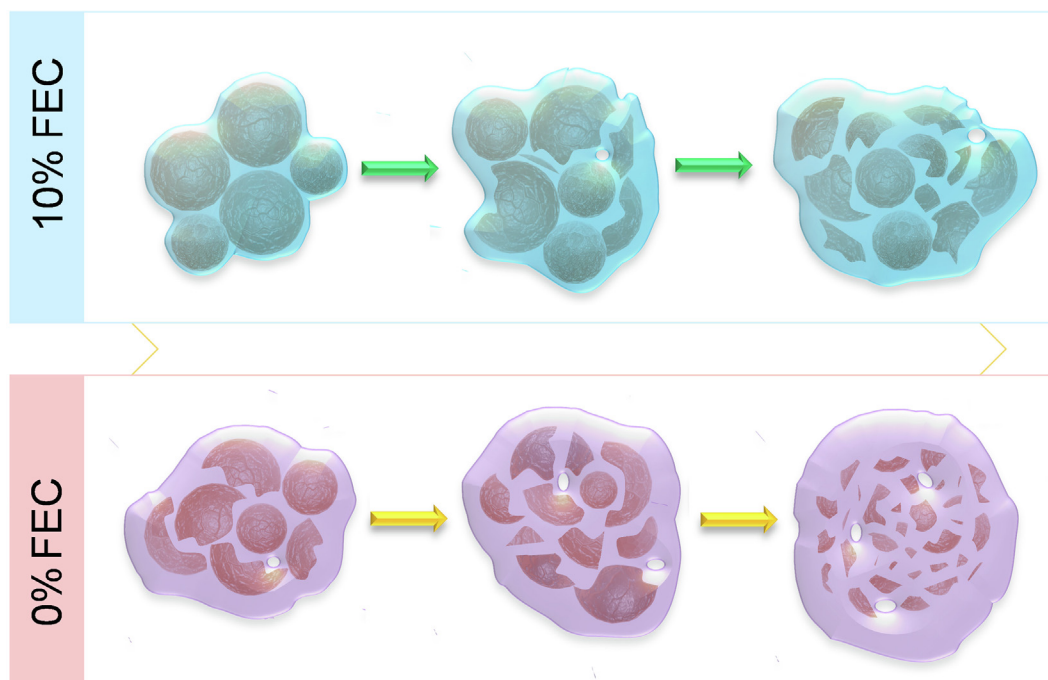


Fig. 6. Schematic diagram of structural evolution in Si anodes with and without FEC additive.

4. Conclusion

In this study, through combining the multi-scale 3D image reconstruction technique and various structure/composition characterization methods, the structural evolution in Si anodes was dissected. The 3D-modeled structural evolution of both Si electrodes and single Si particles were reconstructed by sequential slicing, which enables us to visually and quantitatively identify the dynamic change of active materials, inactive components (e.g., SEI), and voids. From the 3D reconstruction, volume fraction of electrode components and statistical average particles sizes were quantified. It has been revealed that the formation of a stable SEI during early stage of cycling could effectively suppress free volume expansion and particle pulverization in Si anodes, improving the cycle life. Moreover, the methodology presented in this study not only establishes a correlation between the structural evolution of Si anodes and the corresponding electrochemical performance, but also provides a fresh perspective for accurate evaluation of various electrode systems with similar volume expansion during charge/discharge processes (e.g., tin, bismuth).

Conflict of interest

The authors declare that they have no conflict of interest.

Acknowledgment

This work was supported by Soft Science Research Project of Guangdong Province (2017B030301013) and China Postdoctoral Science Foundation (2019M660317).

Author contributions

Zu-Wei Yin, Hai Lin, and Luyi Yang supervised this work. Yinguo Xiao and Feng Pan provided the resources. Chen Zhu and Shiming Chen designed the methodology and analyzed the data with the help of Luyi Yang. Ke Li performed the project administration. Chen

Zhu and Shiming Chen wrote the original draft. Zu-Wei Yin and Luyi Yang reviewed the manuscript. All the authors discussed the results and commented on the manuscript.

Appendix A. Supplementary materials

Supplementary materials to this article can be found online at <https://doi.org/10.1016/j.scib.2023.01.032>.

References

- [1] Tarascon J-M, Armand M. Issues and challenges facing rechargeable lithium batteries. *Nature* 2001;414:359–67.
- [2] Yang L, Yang K, Zheng J, et al. Harnessing the surface structure to enable high-performance cathode materials for lithium-ion batteries. *Chem Soc Rev* 2020;49:4667–80.
- [3] Huang W, Yang L, Chen Z, et al. Elastic lattice enabling reversible tetrahedral Li storage sites in a high-capacity manganese oxide cathode. *Adv Mater* 2022;34:2202745.
- [4] Yang K, Yang L, Wang Z, et al. Constructing a highly efficient aligned conductive network to facilitate depolarized high-areal-capacity electrodes in Li-ion batteries. *Adv Energy Mater* 2021;11:2100601.
- [5] Li JY, Xu Q, Li G, et al. Research progress regarding Si-based anode materials towards practical application in high energy density Li-ion batteries. *Mater Chem Front* 2017;1:1691–708.
- [6] Yang YF, Yang JL, Pan F, et al. From intercalation to alloying chemistry: structural design of silicon anodes for the next generation of lithium-ion batteries. *Chinese J Struct Chem* 2020;39:16–9.
- [7] Chen S, Song Z, Wang L, et al. Establishing a resilient conductive binding network for Si-based anodes via molecular engineering. *Acc Chem Res* 2022;55:2088–102.
- [8] Chan CK, Peng H, Liu G, et al. High-performance lithium battery anodes using silicon nanowires. *Nat Nanotechnol* 2008;3:31–5.
- [9] Michan AL, Divitini G, Pell AJ, et al. Solid electrolyte interphase growth and capacity loss in silicon electrodes. *J Am Chem Soc* 2016;138:7918–31.
- [10] Haregewoin AM, Wotango AS, Hwang BJ. Electrolyte additives for lithium ion battery electrodes: progress and perspectives. *Energy Environ Sci* 2016;9:1955–88.
- [11] Rezqita A, Sauer M, Foelske A, et al. The effect of electrolyte additives on electrochemical performance of silicon/mesoporous carbon (Si/MC) for anode materials for lithium-ion batteries. *Electrochim Acta* 2017;247:600–9.
- [12] Hu J, Ji Y, Zheng G, et al. Influence of electrolyte structural evolution on battery applications: cationic aggregation from dilute to high concentration. *Aggregate* 2022;3:e153.

- [13] Etacheri V, Haik O, Goffer Y, et al. Effect of fluoroethylene carbonate (FEC) on the performance and surface chemistry of Si-nanowire Li-ion battery anodes. *Langmuir* 2012;28:965–76.
- [14] Nie M, Demeaux J, Young BT, et al. Effect of vinylene carbonate and fluoroethylene carbonate on SEI formation on graphitic anodes in Li-ion batteries. *J Electrochem Soc* 2015;162:A7008–14.
- [15] Schroder K, Alvarado J, Yersak TA, et al. The effect of fluoroethylene carbonate as an additive on the solid electrolyte interphase on silicon lithium-ion electrodes. *Chem Mater* 2015;27:5531–42.
- [16] Zhang Q, Pan J, Lu P, et al. Synergetic effects of inorganic components in solid electrolyte interphase on high cycle efficiency of lithium ion batteries. *Nano Lett* 2016;16:2011–6.
- [17] Zhang X, Weng S, Yang G, et al. Interplay between solid-electrolyte interphase and (in)active Li_xSi in silicon anode. *Cell Reports Phys Sci* 2021;2:100668.
- [18] Chen S, Wang Z, Wang L, et al. Constructing a robust solid-electrolyte interphase layer via chemical prelithiation for high-performance SiO_x anode. *Adv Energy Sustain Res* 2022;3:2200083.
- [19] Huang W, Wang J, Braun MR, et al. Dynamic structure and chemistry of the silicon solid-electrolyte interphase visualized by cryogenic electron microscopy. *Matter* 2019;1:1232–45.
- [20] Surace Y, Leanza D, Mirollo M, et al. Evidence for stepwise formation of solid electrolyte interphase in a Li-ion battery. *Energy Storage Mater* 2022;44:156–67.
- [21] Ebner M, Marone F, Stampanoni M, et al. Visualization and quantification of electrochemical and mechanical. *Science* 2013;342:716–21.
- [22] Lu X, Bertei A, Finegan DP, et al. 3D microstructure design of lithium-ion battery electrodes assisted by X-ray nano-computed tomography and modelling. *Nat Commun* 2020;11:2079.
- [23] Wang Z, Ke X, Zhou K, et al. Engineering the structure of ZIF-derived catalysts by revealing the critical role of temperature for enhanced oxygen reduction reaction. *J Mater Chem A* 2021;9:18515–25.
- [24] Ercius P, Alaidi O, Rames MJ, et al. Electron tomography: a three-dimensional analytic tool for hard and soft materials research. *Adv Mater* 2015;27:5638–63.
- [25] Lee KT, Vito NJ, Wachsman ED. Comprehensive quantification of Ni-Gd_{0.1}Ce_{0.9}O_{1.95} anode functional layer microstructures by three-dimensional reconstruction using a FIB/SEM dual beam system. *J Power Sources* 2013;228:220–8.
- [26] Gaiselmann G, Neumann M, Holzer L, et al. Stochastic 3D modeling of La_{0.6}St_{0.4}CoO_{3-δ} cathodes based on structural segmentation of FIB-SEM images. *Comput Mater Sci* 2013;67:48–62.
- [27] Ambrose RJ, Hartman RC, Labs W, et al. Shale gas-in-place calculations part i: new pore-scale considerations. *SPE J* 2012;17:219–29.
- [28] Liu X, Zheng B, Zhao J, et al. Electrochemo-mechanical effects on structural integrity of Ni-rich cathodes with different microstructures in all solid-state batteries. *Adv Energy Mater* 2021;11:202003583.
- [29] Scharf J, Chouchane M, Finegan DP, et al. Bridging nano- and microscale X-ray tomography for battery research by leveraging artificial intelligence. *Nat Nanotechnol* 2022;17:446–59.
- [30] Jang J, Kang I, Choi J, et al. Molecularly tailored lithium-arene complex enables chemical prelithiation of high-capacity lithium-ion battery anodes. *Angew Chemie Int Ed* 2020;59:14473–80.
- [31] Wan TH, Saccoccio M, Chen C, et al. Influence of the discretization methods on the distribution of relaxation times deconvolution: implementing radial basis functions with drttools. *Electrochim Acta* 2015;184:483–99.
- [32] Lu Y, Zhao CZ, Huang JQ, et al. The timescale identification decoupling complicated kinetic processes in lithium batteries. *Joule* 2022;6:1172–98.
- [33] Hahn M, Schindler S, Triebels LC, et al. Optimized process parameters for a reproducible distribution of relaxation times analysis of electrochemical systems. *Batteries* 2019;5:43–63.
- [34] Li L, Fang C, Wei W, et al. Nano-ordered structure regulation in delithiated Si anode triggered by homogeneous and stable Li-ion diffusion at the interface. *Nano Energy* 2020;72:104651.
- [35] Soni R, Robinson JB, Shearing PR, et al. Lithium-sulfur battery diagnostics through distribution of relaxation times analysis. *Energy Storage Mater* 2022;51:97–107.
- [36] Song B, Sui T, Ying S, et al. Nano-structural changes in Li-ion battery cathodes during cycling revealed by FIB-SEM serial sectioning tomography. *J Mater Chem A* 2015;3:18171–9.
- [37] Almar L, Joos J, Weber A, et al. Microstructural feature analysis of commercial Li-ion battery cathodes by focused ion beam tomography. *J Power Sources* 2019;427:1–14.
- [38] Ender M, Joos J, Carraro T, et al. Quantitative characterization of LiFePO₄ cathodes reconstructed by FIB/SEM tomography. *J Electrochem Soc* 2012;159:A972–80.
- [39] Joos J, Carraro T, Weber A, et al. Reconstruction of porous electrodes by FIB/SEM for detailed microstructure modeling. *J Power Sources* 2011;196:7302–7.
- [40] Yin Y, Arca E, Wang L, et al. Nonpassivated silicon anode surface. *ACS Appl Mater Interfaces* 2020;12:26593–600.
- [41] Jin Y, Kneusels NJH, Marbella LE, et al. Understanding fluoroethylene carbonate and vinylene carbonate based electrolytes for Si anodes in lithium ion batteries with NMR spectroscopy. *J Am Chem Soc* 2018;140:9854–67.
- [42] Markevich E, Salitra G, Chesneau F, et al. Very stable lithium metal stripping-plating at a high rate and high areal capacity in fluoroethylene carbonate-based organic electrolyte solution. *ACS Energy Lett* 2017;2:1321–6.



Chen Zhu received her B.S. degree from Central South University in 2020. She is pursuing her M.S. degree at the School of Advanced Materials, Peking University. Her research interest mainly focuses on characterization methods of lithium-ion battery materials, especially the development and application of in-site observation techniques.



Shiming Chen received his Bachelor's degree from the Institute for Advanced Study, Nanchang University in 2020. He is currently a Ph.D. candidate under the supervision of Prof. Feng Pan at School of Advanced Materials, Peking University Shenzhen Graduate School. His research focuses on the anode materials of lithium-ion batteries and quantum chemical calculation.



Zu-Wei Yin received his Ph.D. degree from Xiamen University in 2019 (Supervision: Prof. Shi-Gang Sun). He is a joint Ph.D. student at Lawrence Berkeley National Lab (USA) between 2016 and 2019 (Supervision: Prof. Haimei Zheng), and a postdoc at Peking University Shenzhen Graduate School between 2019 and 2021 (Supervision: Prof. Feng Pan). He is currently an assistant professor at the College of Energy, Xiamen University. His research interest mainly focuses on the electrochemical energy storage and advanced characterization techniques, such as EQCM, TEM, XAS, etc.



Hai Lin is Vice Dean of School of Advanced Materials, Peking University Shenzhen Graduate School. He is responsible for the testing and characterization platform of new materials, and focusing on the evaluation and industrial application development of clean energy materials and devices.



Luyi Yang received his Bachelor's degree from the Department of Chemistry, Xiamen University in 2010 and earned his Ph.D. degree from the School of Chemistry, Southampton University (UK) in 2015. He is currently an associate research professor at the School of Advanced Materials, Peking University Shenzhen Graduate School. His research interest mainly focuses on the investigation of key materials in lithium batteries.